Flax and hemp composites: Mechanical characterization and numerical modeling

Flax and Hemp Composites: Mechanical Characterization and Numerical Modeling

Part C: Journal of Mechanical Engineering Science
XX(X):1–11

DOI: 10.1177/ToBeAssigned
www.sagepub.com/
SAGE

Giulia Del Bianco [1], Valentina Giammaria [1], Simonetta Boria [1], Dario Fiumarella [2], Raffaele Ciardiello[2], Alessandro Scattina [2], Giovanni Belingardi [2], Vincenzo Castorani [3]

Abstract

Nowadays, in the global composites industry, an increasing number of companies are studying high-quality innovative and green solutions, in order to achieve the environmental sustainability goals. In this context, the use of a natural fiber reinforced polymer in the design of structural components needs to be validated through experimental mechanical tests. This study provides an overview of the behaviors of flax/epoxy and hemp/epoxy laminates subjected to tensile, four-point bending, and Low-Velocity Impact (LVI) tests, both from an experimental and numerical point of view. For each type of test, finite element models were simulated using the explicit code LS-DYNA in order to characterize the materials, reproduce the load-displacement plots, and analyze the damage evolution of the laminates. Two different types of mesh modeling were investigated for the models: shell and solid elements. In both cases, a proper contact modeling between layers was carried out to account for delamination phenomena of the material. The results obtained show an agreement between the experimental response and the simulated one, highlighting the possibility of designing and manufacturing structural components in composite material reinforced with natural fibers.

Keywords

Natural Fiber Composites (NFC), Tensile tests, Four-point bending tests, Low-Velocity Impact (LVI) tests, Finite Element Analysis (FEA).

1 Introduction

In recent years, companies around the world have been striving to develop products and systems that are more sustainable and have less impact on the environment. In this context, the use of natural resources is becoming increasingly important for industry and research, as they prove to be environmentally friendly, such as renewable energies. Natural fibers, in particular, are being explored as potential replacements for the synthetic fibers (e.g., carbon and glass) that are widely used today, typically combined with thermosetting resins. Traditional composites have excellent mechanical properties, such as high strength and stiffness, as well as long life, but they cannot be fully reused or recycled. Therefore, natural fibers are increasingly being studied both as dry materials and as fibers embedded in a matrix, leading to Natural Fiber Composites (NFC).

In the literature, many studies describe the benefits and the critical issues of using natural fibers as reinforcement in polymeric composites: Peças et al.[1], and Neto et al.[2] provided a detailed review in such a way. An analysis on the morphology of natural fibers and their chemical surface modification is well illustrated by Zwawi[3] and Gurunathan et al.[4]. In particular, Yan et al.[5] studied both the chemical structure of flax fibers, together with surface functionalization treatments, and the mechanical properties depending on the fiber configuration, also comparing different types of resins. The mechanical response of NFC is also investigated by Sarikaya et al.[6] and Dhaliwal et al.[7], which provided an experimental and numerical characterization of hemp fiber reinforced composites with epoxy resin. Liang et al.[8] and Caprino et al.[9] provided the results of a Low-Velocity Impact (LVI) test campaign on flax and hemp reinforced composites with epoxy matrix. Panciroli et al.[10] compared the impact resistance of flax/epoxy and glass/epoxy composites through experiments and numerical simulations. In this context, the residual tensile properties and fatigue strength after the impact, related to the damage mechanism, are analyzed by De Vasconcellos et al.[11]. In addition to the most known flax and hemp fibers, there are many other plant-derived fibers that can be found in the literature: some examples are cotton, bamboo, jute, and sisal. The works of Yashas et al.[12] and Ramesh et al.[13] summarized this fibers variety, while Al-Oqla et al.[14] investigated the behavior of the date palm fibers.

Despite many advantages, e.g., low density, non-toxicity, and renewability, natural fibers have some limitations, such as low strength and modulus, high moisture absorption, aging, and easy flammability. To overcome these problems,

[1] School of Science and Technology, Mathematics Division, University of Camerino, Via Madonna delle Carceri 9, 62032 Camerino, Italy
[2] Department of Mechanical and Aerospace Engineering, Politecnico di Torino, Corso Duca degli Abruzzi 24, 10129 Torino, Italy
[3] HP Composites SpA, Dipartimento di Ricerca e Sviluppo, Via del Lampo S.N., Z.Ind.le Campolungo, 63100 Ascoli Piceno, Italy

Corresponding author:
Giulia Del Bianco (G. Del Bianco)
Email: giulia.delbianco@unicam.it

hybridization techniques are considered as solutions to improve the mechanical properties of NFC: synthetic and natural fibers are simultaneously present as reinforcement in the polymer matrix, leading to the formation of a hybrid composite. Partial substitution of synthetic fibers in applications is conceivable, although it will take some time to be mechanically explored and then implemented in large-scale production. In particular, many are the studies focused on the LVI properties and damage characterization of hybrid composites, where the reinforcement was realized combining flax fibers with carbon ones[15–17], and the matrix was epoxy resin. Petrucci et al.[18] compared instead the different behavior of basalt hybridization with flax, hemp and glass fibers. The failure mechanisms of flax fibers have been analyzed in detail by Ahmed et al.[19] and Chapman et al.[15] using Scanning Electron Microscopy (SEM), and it highlight the rearrangement of the fibrils and the fibers pull-out.

Hybrid solutions are already widely used in automotive applications, as shown by the work of Ravishankar et al.[20]. Moreover, Boria et al.[21] presented a case study on the energy absorption capability of impact attenuators for a Formula SAE racing car, analyzing thermoset, thermoplastic and also hybrid configurations. Other applications can be found in wind turbine rotor blades, where the most commonly used raw materials are glass or carbon fibers combined with epoxy resins. A study on new green solutions suitable for the purpose is given by Boria et al.[22], where the analyzed configuration of hemp fibers embedded in vinylester resin is subjected to low-velocity/large-mass impacts.

To comply with European green transition legislations, researchers and industries are exploring new environmental strategies to replace traditional composites with hybrid or fully-green configurations in a variety of applications. The use of NFC could be promising in this sense, both for structural and non-structural components. Moreover, from a Life Cycle Assessment (LCA) perspective, natural fibers ensure a short supply chain, taking into account the cultivation process. In addition to the use of natural fibers, a future goal in terms of sustainability and LCA is also to explore new matrix solutions, such as bio-based epoxy resins produced from agricultural waste and biomass, as described by Väisänen et al.[23]. A crucial challenge is to achieve and maintain a chemically good adhesion between matrix and natural fibers over time - i.e., to improve the so-called fiber/matrix interface - while ensuring good mechanical properties of the final component, depending on the application. In this context, hemp reinforced laminates with bio-based epoxy resin have already been studied in the literature, especially in terms of impact resistance. In the study by Di Landro et al.[24], they were manufactured using Resin Transfer Molding (RTM) injection process and characterized for vibration damping capacity, moisture absorption and fire response. Scarponi et al.[25] instead analyzed their damage resistance and post-impact damage tolerance, when subjected to LVI at different energies up to perforation. In addition, Dhakal et al.[26] investigated the behavior of bio-composites realized with jute fiber reinforcement embedded in methacrylated soybean oil under LVI loading.

In addition to the choice of fiber reinforcement and matrix type, the effect of temperature is also an interesting aspect for predicting material behavior: in this respect, many works in the literature focus on the effects of temperature variations on the impact response of composites[27,28]. In particular, Raponi et al.[29] studied flax/epoxy laminates impacted at -40 °C, room temperature, and 60 °C and presented numerical and analytical models validated on the experimental investigation. Another analytical study was conducted by Boria et al.[30] on the LVI response of hemp and hemp/glass thermoset composites. From these studies, it is clear that both analytical and numerical models can be powerful tools for predicting the mechanical performance of some components and their failure modes, while reducing the number of physical prototypes during the design process. Finite Element (FE) modeling of the progressive crushing phenomenon on components such as tubular absorbers and bumpers using LS-DYNA is well described in the works of Feraboli[31] and Rabiee[32]. In particular, composites realized with flax fibers combined with PLA[33] are numerically analyzed for bumper beams.

Our work fits into this context and represents an initial experimental and numerical analysis of the behavior of green composite laminates, with the aim of providing engineers with a starting point for developing components for a variety of applications. Specifically, the experimental behavior of flax/epoxy and hemp/epoxy laminates during tensile, four-point bending, and LVI tests is investigated in this paper. Numerical modeling of these tests is then performed using the software LS-DYNA[34], where the obtained physical parameters are used in the material models. Depending on the tests, a different approach is taken in the choice of element type - shell or solid - in order to find a compromise with the computational cost of the simulations. Moreover, the trends of the laminates for the tensile tests are better described by using two different material cards, as we will see in Section 5. Finally, the comparison between the experimental and numerical load-displacement plots shows good results that validate the models and provide a good starting point for future and further investigations.

2 Materials

In this work, two different types of natural fiber laminates provided by HP Composites SpA are experimentally investigated and then numerically modeled: one is reinforced with flax, and the other with hemp. Both the configurations are manufactured by stacking 8 layers of a PrePreg with the same orientation. In particular, the two PrePregs are composed of woven reinforcements embedded in the same epoxy resin, and they presents different fiber architectures. The two natural fiber fabrics have the following technical characteristics:

- Flax: balanced twill 2×2, 350 gsm, RC = 38%, FVF = 63%, with 5 threads/cm for the weft and 6 threads/cm for the warp;
- Hemp: unbalanced Turkish satin, 430 gsm, RC = 35%, FVF = 60%, with 5 threads/cm for the weft and 8.5 threads/cm for the warp.

Although the use of balanced fabric in composite laminates is more common in different industries due to the similar properties along the principal axes, unbalanced laminates are

Table 1. Experimental tensile properties of flax and hemp specimens. E: Young modulus; σ_u: ultimate strength; G: shear modulus.

	Orientation	E [GPa]	σ_u [MPa]	G [GPa]
Flax	0°	16.1 ± 0.2	140 ± 16	
	45°	7.3 ± 0.0	80 ± 6	2.2 ± 0.1
	90°	19.5 ± 1.0	163 ± 3	
Hemp	0°	13.4 ± 0.9	117 ± 3	
	45°	7.0 ± 0.1	66 ± 12	2.2 ± 0.0
	90°	21.1 ± 0.2	217 ± 13	

also used in applications where the balance between bending and twisting modes is needed to optimise the mechanical performances of the composite laminates (e.g. wind blades and wings)[35–37].

The curing process is in autoclave at 135 °C and 6 bar for 90 minutes, under a vacuum bag, with an initial heating ramp (rate of 3 °C/min) and a final cooling ramp (rate of 4 °C/min) to ensure uniform temperature distribution and avoid sample deformation. For each reinforcement, the samples present an overall average thickness of 3.68 mm, and the stacking sequences of the plies are respectively $[0]_8$, $[45]_8$, $[90]_8$, depending on the direction in which they are cut, starting from a single plate.

3 Experimental tests

3.1 Tensile and Four-Point Bending tests

For a first characterization of these materials, tensile and four-point bending tests are performed using a servo-hydraulic machine (Instron 8801).

The tensile tests (rectangular specimen dimensions of 250 mm × 25 mm × 3.68 mm) are performed according to the ASTM D3039 standard and considering a test speed of 2 mm/min and a grip pressure of 100 bar. For each material and orientation, three specimens equipped with gauges (type 1-XY38-6/350, from HBM) are tested.

Four-point bending tests (specimen dimensions of 150 mm × 25 mm × 3.68 mm) are performed in accordance with ASTM D6272 with the following setup: a test speed of 2 mm/min, a load span of 30 mm, a support span of 60 mm, so that the ratio of load-to-support span is 1:2. In this case, only the 0° and 90° orientations are considered and four specimens are tested for each orientation.

The tensile and bending properties, i.e. the maximum stress before failure and the elastic and shear moduli, are summarized in Tables 1 and 2, respectively. According to the standard, the Young modulus E is calculated as the slope of the initial linear curve in the stress-strain plot, which corresponds approximately to a strain range between 0.0005 and 0.002. Similarly, the shear modulus G is calculated from the data of the 45° specimens as the slope of the initial linear curve in the shear stress-shear strain plot, in a strain range between 0.001 and 0.004. The flexural modulus E_B is determined from the formula in the standard for a load span of an half of the support span.

Due to the repeatability of these tests, the behavior of a single specimen is taken as a reference for each orientation and configuration tested: Figures 1 and 2 show the stress-strain curves for tensile and bending tests, respectively.

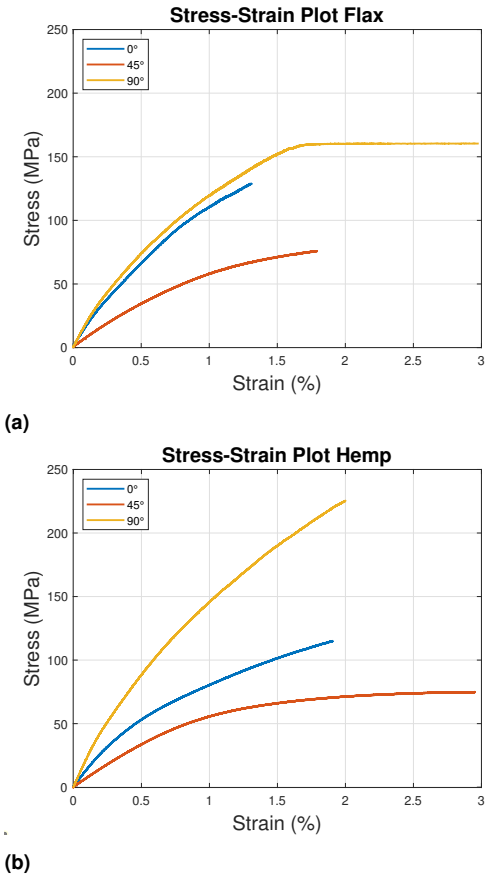

Figure 1. Experimental curves of tensile tests. (a) Flax. (b) Hemp.

Table 2. Experimental flexural properties of flax and hemp specimens. E_B: Flexural modulus; $\sigma_{u,B}$: ultimate flexural strength.

	Orientation	E_B [GPa]	$\sigma_{u,B}$ [MPa]
Flax	0°	12.4 ± 0.8	163 ± 3
	90°	13.3 ± 0.6	168 ± 3
Hemp	0°	10.9 ± 1.2	150 ± 7
	90°	16.4 ± 0.8	198 ± 1

These diagrams illustrate that the mechanical properties of flax and hemp are similar in both tests. In particular, it can be seen that the hemp laminates have better strength and stiffness properties than flax at 90° orientations. This is due to the different architecture of hemp and flax fabric. More precisely, hemp fiber has a higher number of threads/cm along the warp direction than flax, as indicated in Section 2. Hence this greater amount of yarn increases the elastic moduli and strength in that orientation, if compared to the hemp at 0°. On the contrary, the balanced nature of flax laminates is confirmed by the fact that the curves at 0° and 90° are close to each other. This indicates that a proper comparison between these materials is only possible at 0° orientation, where the same number of threads/cm is present. In this particular case, all the experimental results prove the better behavior of flax reinforcement compared to the hemp one. The percentage variations in terms of maximum load between the two materials are presented in Section 5. Moreover, the elastic moduli for both investigated material configurations are higher than the corresponding flexural

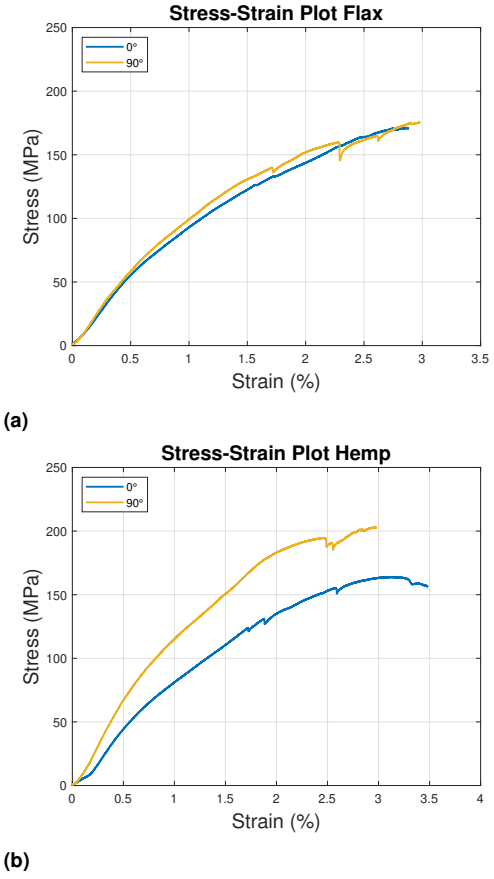

Figure 2. Experimental curves of bending tests. (a) Flax. (b) Hemp.

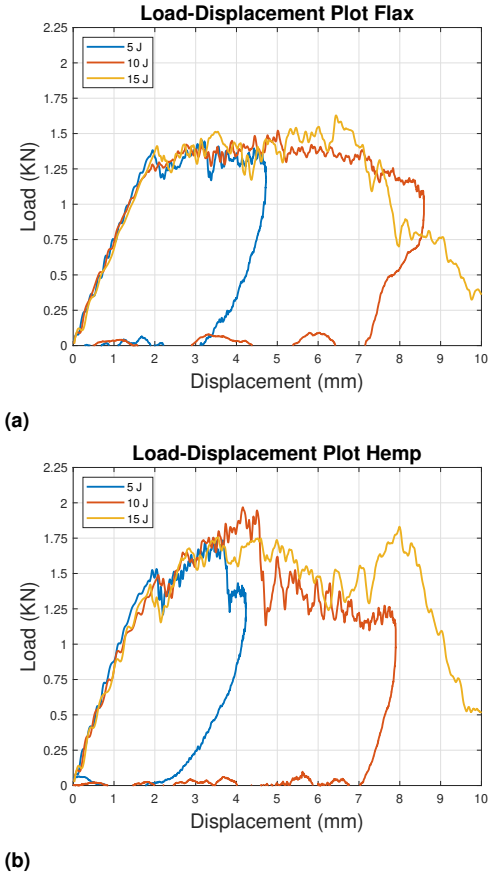

Figure 3. Experimental curves of LVI tests. (a) Flax. (b) Hemp.

moduli, while the stiffness in the flexural tests is higher than in the tensile tests. On the other hand, similarities between the two reinforcements are visible in the failure mechanism: in the stress-strain plots, all the samples show an initial nonlinear behavior, typical of natural fibers, which is related to their viscoelastic nature and the rearrangement of fibrils [19].

3.2 Low-Velocity Impact (LVI) tests

In addition to the mechanical characterization described above, Low-Velocity Impact tests are performed according to the ASTM D5628 standard. Laminate test plates oriented at 0° (100 mm × 100 mm × 3.68 mm) are impacted at three different energy levels: 5 J, 10 J, and 15 J, corresponding to a dart impact velocity of 0.8 m/s, 1.13 m/s, and 1.38 m/s, respectively. A drop tower machine (Instron/CEAST Fractovis Plus) equipped with a hemispherical impactor of 12.7 mm diameter and a total mass of 15.9 kg is used to perform these tests. The different impact energies are evaluated by varying the impactor tip height. The samples are clamped between two steel plates with a circular opening of 40 mm diameter. Five flax and three hemp samples are tested for 10 J, while two samples are tested for the other two energy levels, since the results are repeatable. For this reason, only one load-displacement curve is shown for each energy level in Figures 3a and 3b.

These graphs illustrate that even in this case hemp laminates, despite their lower RC, achieve higher values of maximum load than flax. The experimental impact properties, i.e., the maximum force and the absorbed energy, are summarized in Table 3. Cracking and springback occur at 5 J, wider damage is observed at 10 J, and complete perforation occurs at 15 J.

Visual inspection of the front (Figures 4a and 5a) and the back (Figures 4b and 5b) surfaces shows that both flax and hemp reinforcements exhibit the same failure modes at the three impact energies – i.e., a slight indentation and some circular imprints due to the clamping device on the front surface, and a cross-shaped delamination along the warp and weft direction of the fabric on the back surface. As the impact energy increases, the damage becomes more visible until perforation is reached: in this case, a neat hole marks the samples on the front side, while a sharp failure pattern with cracks along both directions is clearly visible on the back side. This phenomenon is attributed to the high compaction of the plies in the laminates, which allows for a perfectly right-angled failure pattern.

Table 3. Experimental impact properties of flax and hemp specimens. F_{max}: maximum force; E_{ab}: absorbed energy.

	Energy level	$F_{\max}$ [kN]	E_{ab} [J]
Flax	5 J	1.47 ± 0.02	4.18 ± 0.29
	10 J	1.60 ± 0.09	9.67 ± 0.40
	15 J	1.63 ± 0.00	10.56 ± 0.49
Hemp	5 J	1.81 ± 0.08	3.91 ± 0.06
	10 J	1.92 ± 0.04	9.76 ± 0.11
	15 J	1.84 ± 0.01	12.80 ± 0.34

4 Numerical modeling

The Finite Element (FE) models for all the tests described above are initially created using Altair HyperMesh software. Eplicit finite element analyses are then performed with the solver LS-DYNA (release 11.1)[34].

The most commonly used material card for modeling reinforced composites is MAT54/55 (MAT_ENHANCED_COMPOSITE_DAMAGE), which is designed to reproduce the brittle behavior of a unidirectional layer, linear up to failure. Another interesting material model is MAT58 (MAT_LAMINATED_COMPOSITE_FABRIC), since it is developed to simulate the woven fabric composites. For this reason, the authors have chosen to use also the MAT58 material card, although it requires a higher number of parameters than MAT54/55 to perform a simulation. For a detailed description and comparison of the material models available in LS-DYNA to describe the behavior of composite materials, as well as the failure criteria and required parameters, see the manual[34] and the article by Rabiee[32].

The numerical models for the tensile and four-point bending tests are created considering the real specimen dimensions and using shell and solid elements, respectively. For the first test, it is only necessary to model the sample: the boundary condition of prescribed motion is imposed to one edge, while the opposite one is constrained for translations and rotations. For the second test, the supports on which the rectangular specimen rests are included in the model instead. The dimension of the elements is chosen after performing a sensitivity analysis on the mesh size, which showed that square elements of 1 mm side represent the best compromise between precision and computational cost for tensile models. For bending models, two solid elements fully integrated through the thickness are used instead, and the MAT54/55 material model is adopted. Tensile tests are modeled using both MAT54/55 and MAT58 material cards, to show that MAT58 is able to more accurately reproduce the nonlinear behavior of natural fibers in this study, as confirmed by the results in Section 5.

The numerical model for the LVI tests, shown in Figure 6, consists of 4 composite shell layers (PART_COMPOSITE),

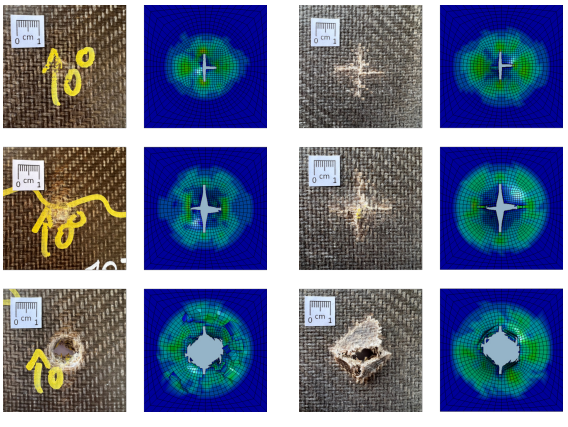

Figure 4. Experimental and numerical damage progression on flax/epoxy laminates surfaces impacted at different energy levels. (a) Front. (b) Back.

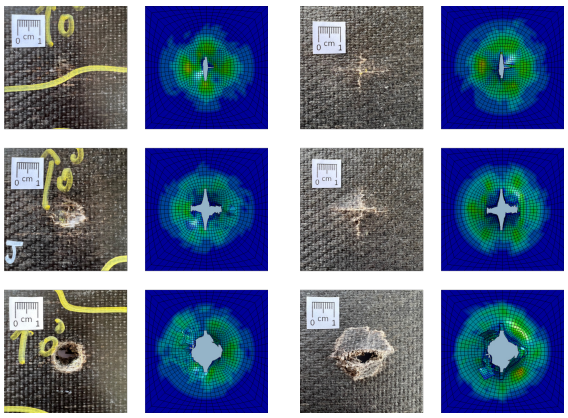

Figure 5. Experimental and numerical damage progression on hemp/epoxy laminates surfaces impacted at different energy levels. (a) Front. (b) Back.

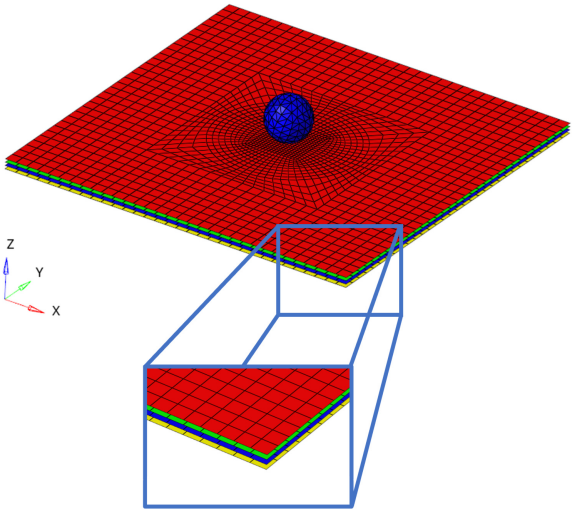

Figure 6. Numerical impact model, with a close-up of the four layers.

each of which with 2 integration points through the thickness to reproduce the 8 layers of the real specimens. Boundary conditions are prescribed to the nodes outside the impact zone: translations and rotations are locked, so that all the degrees of freedom are constrained.

The spherical impactor is modeled as a rigid body with solid elements using the MAT20 (MAT_RIGID) material card. The total mass is equal to that of the experimental test and it is assigned to the sphere. The behavior of the composites is described using the MAT54/55 (MAT_ENHANCED_COMPOSITE_DAMAGE) material model, according to the experimental values presented in Section 3. The total thickness of the 8 plies is 3.68 mm, so each modeled ply is 0.46 mm thick. To reduce simulation times, a finer mesh (with an element size of 1 mm) is used for the square central impact zone, while a gradually coarser mesh is chosen for the rest of the region, since the laminates outside the central region are generally subjected to a lower stress state and therefore do not require the same mesh refinement. In addition, a proper contact modeling need to be defined to reproduce the delamination between the plies: first, one

contact (CONTACT_SURFACE_TO_SURFACE) is imposed between the impactor and the laminates to analyze the interaction between the master and slave surfaces during the impact. Then, three tie-break contacts (CONTACT_AUTOMATIC_ONE_WAY_SURFACE_TO_SURFACE_TIEBREAK) connect the 4 modeled layers and describe their interlaminar interactions[38]. Finally, the three initial impactor velocities corresponding to the tested energy levels are set as initial conditions for the sphere, while all nodes outside the impact zone are constrained by interlocking. Therefore, the same model is used for both materials and for all impact energy cases, changing only the initial velocity of the sphere and the properties of the material card.

5 Results and discussion

In this section the experimental trends are compared with the numerical ones. In the same order as in Section 3, the results of the numerical tensile model for each orientation and material are shown in Figures 7 and 8. From these plots, it can be seen that flax laminates achieve higher force values at 0° and 45° than unbalanced hemp ones (20.1% and 6.8%, respectively), although they reach almost the same displacement at failure. In contrast, the hemp composites show better behavior at 90° and can withstand 20.1% higher load. The opposite tendency of the results is due to the fact that hemp fabric is an unbalanced Turkish satin, as already discussed in Sections 2 and 3, and is therefore much more resistant in the transverse direction than in the longitudinal one.

The numerical model is validated for both materials, and it appears from the graphs that the trend obtained with the MAT54/55 material card – represented by the black curves in Figures 7 and 8 – is not so accurate to reproduce the nonlinear behavior typical of the natural fiber composite laminates. As mentioned earlier, the MAT54/55 material model is designed to reproduce a unidirectional fiber composite, that exhibits a linear behavior until fracture, typical of brittle materials. Except for the values obtained from the experimental campaign, the other parameters in Tables 4 and 5 are selected by a trial-and-error procedure. In particular, we refer to the maximum matrix strain for fiber tension and compression (DFAILM), the maximum shear strain (DFAILS), the maximum strain for fiber tension (DFAILT) and compression (DFAILC), and the longitudinal compressive strength (XC). DFAILM, DFAILC and XC are not available from our experimental campaign, while DFAILT and DFAILS strongly affect the results. Their experimentally derived values are too small in this particular case because the architecture of our samples is a woven fabric (i.e., Twill 2×2 and Turkish satin) and the MAT54/55 is defined for UD fibers. For this reason, DFAILM assumes the same role as DFAILT, but in the transverse direction. On the other hand, MAT58 material card is created to model woven fiber composite materials and is therefore better able to reproduce the elasto-plastic trend of natural fibers in the load-displacement plots, as we can see from the red dashed curves in Figures 7 and 8. They show the good visible results, in agreement with the experimental ones, and confirm that MAT58 material card could be a powerful tool to reproduce the behavior of NFC, and therefore it deserves further investigation. In this particular case, all the parameters used in the numerical simulations of the tensile tests are listed in Tables 6 and 7. They are experimentally derived, except for the stress limit (TAU1) and the strain limit (GAMMA1) of the first slightly nonlinear part of the shear stress-shear strain curve, and the maximum effective strain for element layer failure (ERODS), which again are determined by trial and error. Moreover, it is worth to note that the longitudinal and transverse compressive stress (XC, YC) and strain (E11C, E22C) do not play a role in a tensile test modeling; therefore, they should be accurately selected when modeling other tests.

Table 4. MAT54/55 Material properties for flax laminates. Moduli and strengths are expressed in GPa, density in Kg/mm^3.

MAT_ENHANCED_COMPOSITE_DAMAGE (MAT54/55)				
RO	**EA**	**EB**	**PRBA**	
1.29 E-6	10.3	10.3	0.17	
GAB	**GBC**	**GCA**		
1.8	0.3	0.3		
DFAILM	**DFAILS**	**DFAILT**	**DFAILC**	
0.105623	0.2	0.0885269	-0.0626081	
XC	**XT**	**YC**	**YT**	**SC**
0.2	0.12	0.2	0.12	0.0304

Table 5. MAT54/55 Material properties for hemp laminates. Moduli and strengths are expressed in GPa, density in Kg/mm^3.

MAT_ENHANCED_COMPOSITE_DAMAGE (MAT54/55)				
RO	**EA**	**EB**	**PRBA**	
1.33 E-6	6.5	14.2	0.14	
GAB	**GBC**	**GCA**		
2.0	0.3	0.3		
DFAILM	**DFAILS**	**DFAILT**	**DFAILC**	
0.108	0.21	0.081	-0.095	
XC	**XT**	**YC**	**YT**	**SC**
0.29	0.127	0.29	0.145	0.033

Table 6. MAT58 Material properties for flax laminates. Moduli and strengths are expressed in GPa, density in Kg/mm^3.

MAT_LAMINATED_COMPOSITE_FABRIC (MAT58)				
RO	**EA**	**EB**	**PRBA**	
1.29 E-6	10.3	10.3	0.17	
TAU1	**GAMMA1**	**FS**		
40	0.035	-1		
GAB	**GBC**	**GCA**	**ERODS**	
1.8	0.3	0.3	0.03	
E11C	**E11T**	**E22C**	**E22T**	**GMS**
0.06	0.0234	0.06	0.0234	0.0417
XC	**XT**	**YC**	**YT**	**SC**
0.2	0.14	0.2	0.16	0.04

Table 7. MAT58 Material properties for hemp laminates. Moduli and strengths are expressed in GPa, density in Kg/mm^3.

MAT_LAMINATED_COMPOSITE_FABRIC (MAT58)				
RO	**EA**	**EB**	**PRBA**	
1.33 E-6	6.5	14.2	0.14	
TAU1	**GAMMA1**	**FS**		
35	0.035	-1		
GAB	**GBC**	**GCA**	**ERODS**	
2.2	0.3	0.3	0.035	
E11C	**E11T**	**E22C**	**E22T**	**GMS**
0.06	0.035	0.06	0.035	0.035
XC	**XT**	**YC**	**YT**	**SC**
0.2	0.12	0.2	0.22	0.033

Table 8. Automatic one way surface-to-surface tiebreak contact properties. The omitted parameters are default values.

ONE_WAY_SURFACE_TO_SURFACE_TIEBREAK			
FS	**FD**		
0.1	0.1		
OPTION	**NFLS**	**SFLS**	**PARAM**
8	0.005	0.007	0.15

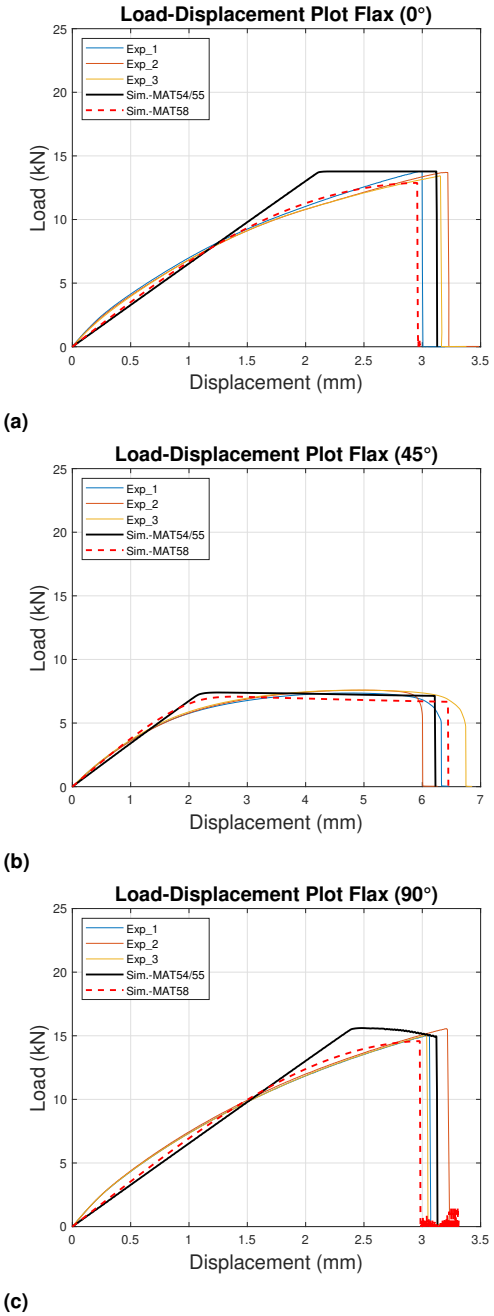

Figure 7. Comparison between experimental and numerical curves of tensile tests for flax samples oriented at (a) 0°, (b) 45° and (c) 90°.

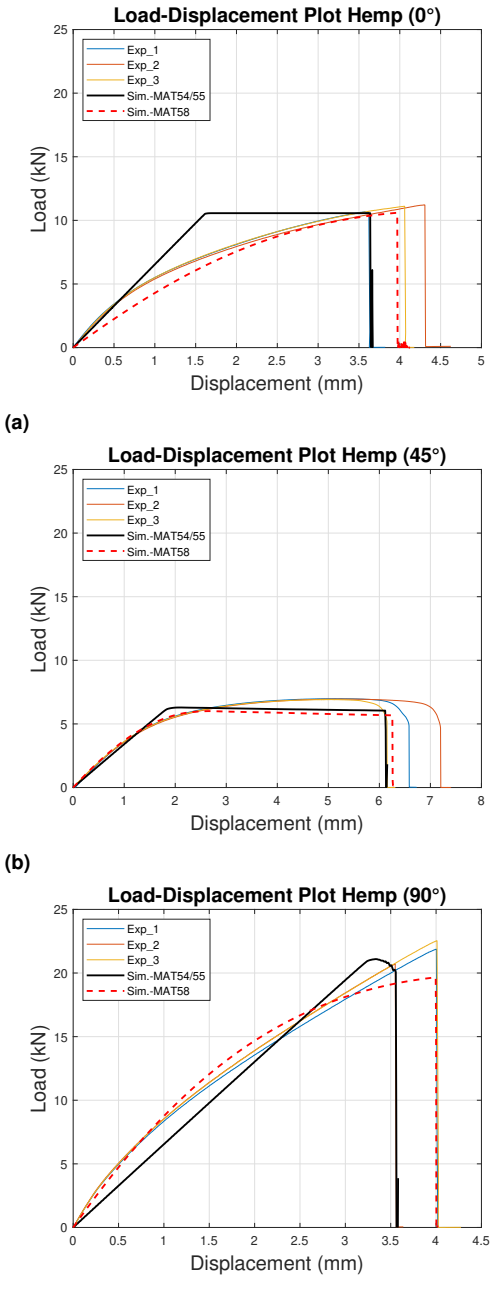

Figure 8. Comparison between experimental and numerical curves of tensile tests for hemp samples oriented at (a) 0°, (b) 45° and (c) 90°.

On the other hand, as mentioned in Section 4, the numerical model for the four-point bending tests is created considering only the MAT54/55 material card. In contrast to the tensile tests, the model in this case is able to reproduce the experimental load-displacement trend well, as confirmed by Figures 9 and 10. These plots once again illustrate the similar mechanical properties of the two materials for the 0° orientation (Figures 9a and 10a, where the flax achieves a 4.8% higher load than hemp), and the greater flexural strength of the hemp laminates in the transverse direction (Figure 10b, with a maximum force 18.1% higher than flax).

Finally, as far as the LVI tests are concerned, it is evident from Figures 11 and 12 that also in this case the MAT54/55 material model is able to reproduce well the experimental trend for both analyzed material configurations. Table 8 summarizes the properties of the tiebreak contact that connects the modeled layers. The comparison of the graphs shows that, regardless of the impact energy, all curves are characterized by a first linear-elastic phase representing the stiffness of the material, which is comparable for the configurations involved. On the contrary, hemp laminates

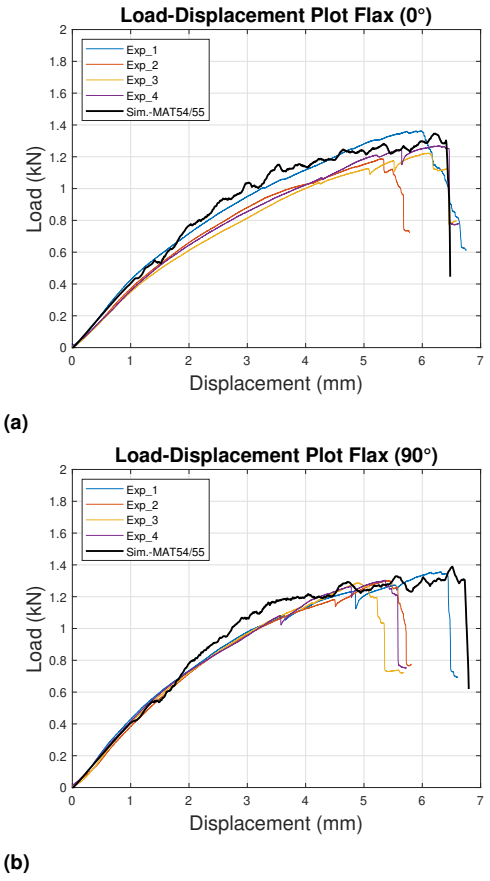

Figure 9. Comparison between experimental and numerical curves of four-point bending tests for flax samples oriented at (a) 0° and (b) 90°.

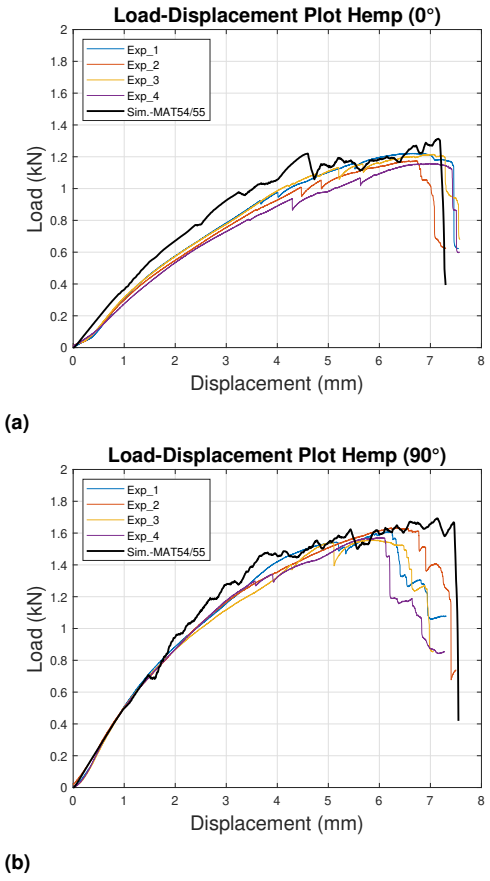

Figure 10. Comparison between experimental and numerical curves of four-point bending tests for hemp samples oriented at (a) 0° and (b) 90°.

show more unstable behavior with load peaks compared to flax, whose load tends to remain constant. While both materials achieve comparable displacement values at the same energy level, the hemp laminates reach higher force values than the flax laminates at all three impact energies (18.8% at 5 J, 16.7% at 10 J, and 11.4% at 15 J, respectively). The explanation for this result can again be attributed to the unbalanced nature of the hemp fabric, illustrating that an unbalanced laminate paradoxically provides better results in terms of strength and energy absorption than a balanced one. Except for impacts at 15 J, the load-displacement curves show a closed loop pattern, which means that part of the elastic energy is given back to the impactor, leading to its rebound[25,30]. Global deformation, delamination, fiber breakage and matrix cracking are the main fracture phenomena. Figures 4 and 5 illustate the comparison between the experimental and the corresponding numerical damage on the front and the back surfaces, for flax and hemp respectively.

6 Conclusions

This study provides an overview of the initial investigation of flax/epoxy and hemp/epoxy laminates in terms of mechanical characterization and numerical modeling, with the aim of exploring their potential as substitutes for synthetic fibers.

A broad equivalence of the properties of the two analyzed material configurations is established through a complete experimental campaign that includes tensile, four-point bending, and LVI tests. Subsequently, FE modeling and analysis are performed for each of these tests using shell or solid elements to capture the delamination phenomenon where possible. As described in Section 5, the numerical curves are aligned with the experimental ones and the sample failure is well reproduced. Furthermore, the damage propagation is correctly reproduced by the impact models.

The application of natural fibers as reinforcement in composites for structural components requires a comprehensive research study that includes a more in-depth analysis, for example, regarding the energy absorption of the samples. These aspects will be investigated in the future, together with the mechanical characterization of hybrid laminates embedded in a toughened epoxy resin.

Declaration of conflicting interests

The authors declare that there is no conflict of interest.

Data availability

The data required to reproduce the results cannot be shared at this time because they are part of an ongoing study.

References

1. Peças P, Carvalho H, Salman H, et al. Natural fibre composites and their applications: a review. *Journal of Composites Science* 2018; 2(4): 66. doi:10.3390/jcs2040066.

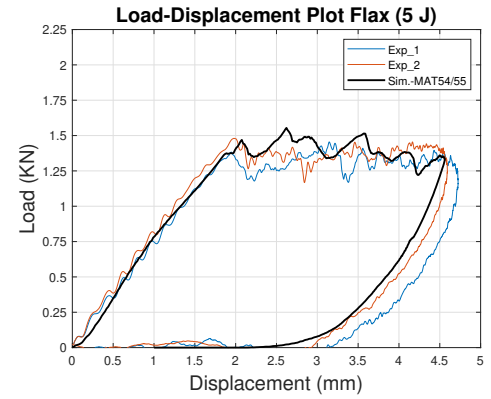

(a)

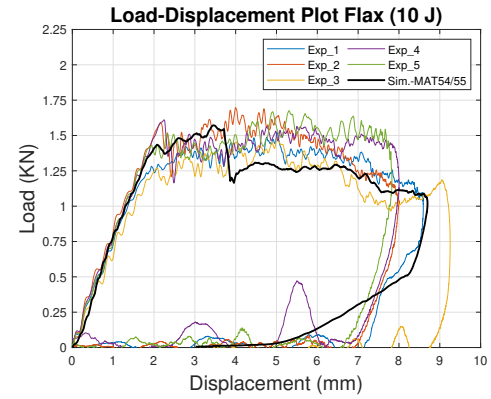

(b)

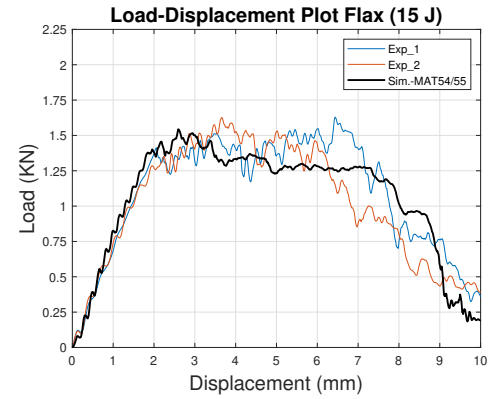

(c)

Figure 11. Comparison between experimental and numerical curves of LVI tests for flax samples impacted at (a) 5 J, (b) 10 J and (c) 15 J.

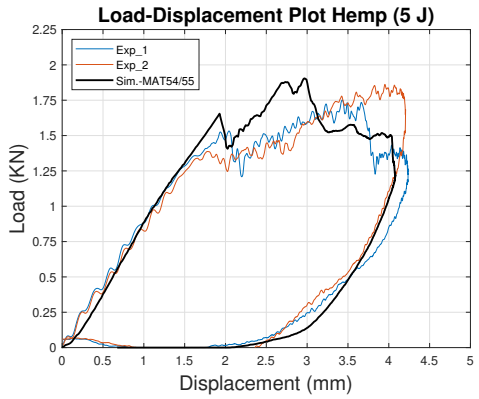

(a)

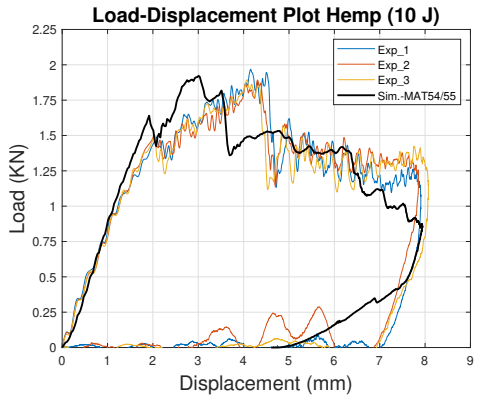

(b)

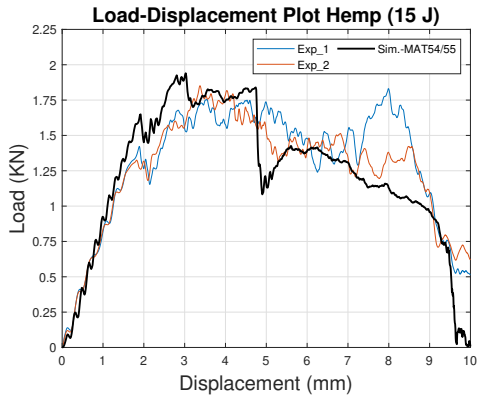

(c)

Figure 12. Comparison between experimental and numerical curves of LVI tests for hemp samples impacted at (a) 5 J, (b) 10 J, and (c) 15 J.

2. Neto J, Queiroz H, Aguiar R, et al. A review of recent advances in hybrid natural fiber reinforced polymer composites. *Journal of Renewable Materials* 2022; 10(3): 561–589. doi:10.32604/jrm.2022.017434.
3. Zwawi M. A review on natural fiber bio-composites, surface modifications and applications. *Molecules* 2021; 26(2): 404. doi:10.3390/molecules26020404.
4. Gurunathan T, Mohanty S and Nayak SK. A review of the recent developments in biocomposites based on natural fibres and their application perspectives. *Composites Part A: Applied Science and Manufacturing* 2015; 77: 1-25. doi:10.1016/j.compositesa.2015.06.007.
5. Yan L, Chouw N and Jayaraman K. Flax fibre and its composites – A review. *Composites Part B: Engineering* 2014; 56: 296-317. doi:10.1016/j.compositesb.2013.08.014.
6. Sarikaya E, Çallioğlu H and Demirel H. Production of epoxy composites reinforced by different natural fibers and their mechanical properties. *Composites Part B: Engineering* 2019; 167: 461–466. doi:10.1016/j.compositesb.2019.03.020.
7. Dhaliwal GS, Dueck SM and Newaz GM. Experimental and numerical characterization of mechanical properties of hemp fiber reinforced composites using multiscale analysis approach. *SN Applied Sciences* 2019; 1: 1361. doi:10.1007/s42452-019-1383-6.
8. Liang S, Guillaumat L and Gning PB. Impact behaviour of flax/epoxy composite plates. *International Journal of Impact Engineering* 2015; 80: 56-64. doi:10.1016/j.ijimpeng.2015.01.006.

9. Caprino G, Carrino L, Durante M, et al. Low impact behaviour of hemp fibre reinforced epoxy composites. *Composite Structures* 2015; 133: 892-901. doi:10.1016/j.compstruct.2015.08.029.
10. Panciroli R and Giannini O. Comparing the impact resistance of flax/epoxy and glass/epoxy composites through experiments and numerical simulations *Composite Structures* 2021; 264; 113750. doi:10.1016/j.compstruct.2021.113750.
11. De Vasconcellos DS, Sarasini F, Touchard F, et al. Influence of low velocity impact on fatigue behaviour of woven hemp fibre reinforced epoxy composites. *Composites: Part B* 2014; 66: 46-57. doi:10.1016/j.compositesb.2014.04.025.
12. Yashas Gowda TG, Sanjay MR, Jyotishkumar P, et al. Natural fibers as sustainable and renewable resource for development of eco-friendly composites: a comprehensive review. *Frontiers in Materials* 2019; 6: 226. doi:10.3389/fmats.2019.00226.
13. Ramesh M, Palanikumar K and Hemachandra Reddy K. Plant fibre based bio-composites: sustainable and renewable green materials. *Renewable and Sustainable Energy Reviews* 2017; 79: 558-584. doi:10.1016/j.rser.2017.05.094.
14. Al-Oqla FM and Sapuan SM. Natural fiber reinforced polymer composites in industrial applications: feasibility of date palm fibers for sustainable automotive industry. *Journal of Cleaner Production* 2014; 66: 347-354. doi:10.1016/j.jclepro.2013.10.050.
15. Chapman M and Dhakal HN. Effects of hybridisation on the low velocity falling weight impact and flexural properties of flax-carbon/epoxy hybrid composites. *Fibers* 2019; 7(11): 95. doi:10.3390/fib7110095.
16. Sarasini F, Tirillò J, D'Altilia S, et al. Damage tolerance of carbon/flax hybrid composites subjected to low velocity impact. *Composites Part B: Engineering* 2016, 91; 144-153. doi:10.1016/j.compositesb.2016.01.050.
17. Al-Hajaj Z, Sy BL, Bougherara H, et al. Impact properties of a new hybrid composite material made from woven carbon fibres plus flax fibres in an epoxy matrix. *Composite Structures* 2019; 208: 346-356. doi:10.1016/j.compstruct.2018.10.033.
18. Petrucci R, Santulli C, Puglia D, et al. Impact and post-impact damage characterisation of hybrid composite laminates based on basalt fibres in combination with flax, hemp and glass fibres manufactured by vacuum infusion. *Composites Part B: Engineering* 2015; 69: 507-515. doi:10.1016/j.compositesb.2014.10.031.
19. Ahmed S and Ulven CA. Dynamic in-situ observation on the failure mechanism of flax fiber through Scanning Electron Microscopy. *Fibers* 2018; 6(1):17. doi:10.3390/fib6010017.
20. Ravishankar B, Nayak SK and Kader MA. Hybrid composites for automotive applications – A review. *Journal of Reinforced Plastics and Composites* 2019; 38(18): 835-845. doi:10.1177/0731684419849708.
21. Boria S, Belingardi G and Scattina A. Thermosetting and thermoplastic impact attenuator under axial loading. *Multiscale and Multidisciplinary Modeling, Experiments and Design* 2019; 2: 129–139. doi:10.1007/s41939-018-0037-5.
22. Boria S, Santulli C, Raponi E, et al. Evaluation of a new green composite solution for wind turbine blades. *Multiscale and Multidisciplinary Modeling, Experiments and Design* 2019; 2: 141–150. doi:10.1007/s41939-019-00043-4.
23. Väisänen T, Das O and Tomppo L. A review on new bio-based constituents for natural fiber-polymer composites. *Journal of Cleaner Production* 2017; 149: 582-596. doi:10.1016/j.jclepro.2017.02.132.
24. Di Landro L and Janszen G. Composites with hemp reinforcement and bio-based epoxy matrix. *Composites Part B: Engineering* 2014; 67: 220-226. doi:10.1016/j.compositesb.2014.07.021.
25. Scarponi C, Sarasini F, Tirillò J, et al. Low-velocity impact behaviour of hemp fibre reinforced bio-based epoxy laminates. *Composites Part B: Engineering* 2016; 91: 162-168. doi:10.1016/j.compositesb.2016.01.048.
26. Dhakal HN, Skrifvars M, Adekunle K, et al. Falling weight impact response of jute/methacrylated soybean oil bio-composites under low velocity impact loading. *Composites Science and Technology* 2014; 92: 134-141. doi:10.1016/j.compscitech.2013.12.014.
27. Suresh Kumar C, Arumugam V, Dhakal HN, et al. Effect of temperature and hybridisation on the low velocity impact behavior of hemp-basalt/epoxy composites *Composite Structures* 2015; 125: 407–416. doi:10.1016/j.compstruct.2015.01.037.
28. Sápi Z and Butler R. Properties of cryogenic and low temperature composite materials – A review. *Cryogenics* 2020; 111: 103190. doi:10.1016/j.cryogenics.2020.103190.
29. Raponi E, Sergi C, Boria S, et al. Temperature effect on impact response of flax/epoxy laminates: analytical, numerical and experimental results. *Composite Structures* 2021; 274: 114316. doi:10.1016/j.compstruct.2021.114316.
30. Boria S, Santulli C, Raponi E, et al. Analytical modeling and experimental validation of the low-velocity impact response of hemp and hemp/glass thermoset composites. *Journal of Composite Materials* 2019; 54(3): 409-421. doi:10.1177/0021998319862856.
31. Feraboli P, Wade B, Deleo F, et al. LS-DYNA MAT54 modeling of the axial crushing of a composite tape sinusoidal specimen. *Composites Part A: Applied Science and Manufacturing* 2011; 42: 1809-1825. doi:10.1016/j.compositesa.2011.08.004.
32. Rabiee A and Ghasemnejad H. Finite Element Modelling approach for progressive crushing of composite tubular absorbers in LS-DYNA: review and findings. *Journal of Composites Science* 2022; 6(1): 11. doi:10.3390/jcs6010011.
33. Jiao-Wang L, Loya JA and Santiuste C. On the numerical modeling of flax/PLA bumper beams. *Materials* 2022; 15(16): 5480. doi:10.3390/ma15165480.
34. LS-DYNA Keyword User's Manual. Vol II, Material Models, R13 ed. Livermore Software Technology, 2021. https://www.dynasupport.com/manuals/ls-dyna-manuals/ls-dyna_manual_volume_ii_r13.pdf
35. Shakya P, Sunny MR and Maiti DK. A parametric study of flutter behavior of a composite wind turbine blade with bend-twist coupling. *Composite Structures* 2019; 207: 764-775. doi:10.1016/j.compstruct.2018.09.064.
36. Hayat K and Ha SK. Load mitigation of wind turbine blade by aeroelastic tailoring via unbalanced laminates composites. *Composite Structures* 2015; 128: 122-133. doi:10.1016/j.compstruct.2015.03.042.
37. Krüger WR, Dillinger J, De Breuker R, et al. Investigations of passive wing technologies for load reduction. *CEAS Aeronautical Journal* 2019; 10: 977-993. doi:10.1007/s13272-019-00393-2.
38. Dogan F, Hadavinia H, Donchev T, et al. Delamination of impacted composites structures by cohesive zone interface

elements and tiebreak contact. *Central European Journal of Engineering* 2012; 2: 612-626. doi:10.2478/s13531-012-0018-0.